Available online at www.sciencedirect.com
ScienceDirect
Trans. Nonferrous Met. Soc. China 32(2022) 134−146
Transactions of Nonferrous Metals Society of China
www.tnmsc.cn

Microstructure and corrosion behavior of as-homogenized and as-extruded Mg−*x*Li−3Al−2Zn−0.5Y alloys (*x*=4, 8, 12)

Xiang PENG, Jia-wei SUN, Hong-jie LIU, Guo-hua WU, Wen-cai LIU

National Engineering Research Center of Light Alloy Net Forming and State Key Laboratory of Metal Matrix Composite, School of Materials Science and Engineering, Shanghai Jiao Tong University, Shanghai 200240, China

Received 16 November 2021; accepted 28 December 2021

Abstract: The microstructure and corrosion behavior of the as-homogenized and as-extruded Mg−*x*Li−3Al−2Zn−0.5Y alloys (*x*=4, 8, 12, wt.%) were studied. The results show that as the Li content increases from 4% to 12%, the matrix transfers from single *α*-Mg phase, (*α*-Mg+*β*-Li) dual phase to single *β*-Li phase. A mixed corrosion feature of intergranular corrosion and pitting corrosion occurs in the Mg−4Li−3Al−2Zn−0.5Y and Mg−12Li−3Al−2Zn−0.5Y alloys. The former is related to the precipitated AlLi phase along the grain boundaries, and the latter is related to the high potential difference between the second phase and the matrix. The corrosion resistance of the as-extruded alloys is better than that of the as-homogenized alloys. The superior corrosion resistance of the as-extruded Mg−8Li−3Al−2Zn−0.5Y alloy with the lowest corrosion rate (P_W=(0.63±0.26) mm/a) is attributed to the more uniform distribution of second phases, the protective *α*-Mg phase via sacrificing the *β*-Li phase and the relatively integrated oxide film.

Key words: Mg−*x*Li−3Al−2Zn−0.5Y alloys; microstructure; corrosion behavior; homogenization; extrusion; second phase; oxide film

1 Introduction

Because of the high specific strength, specific stiffness, excellent machining performance and good damping capacity, Mg−Li alloys as the lightest structure materials can be widely used in the military, aerospace, anode materials and biological fields. The addition of Li element can weaken the *c*/*a* ratio of Mg lattice and change the crystal structure from hexagonal close packed (HCP) to body centered cubic (BCC), therefore improving the deformation ability of Mg alloys [1−3]. However, the high chemical activities of Mg and Li elements accelerate the inner corrosion of Mg−Li alloys, therefore limiting the development and practical application of Mg−Li based alloys [4,5].

The microstructure of Mg alloys plays a significant role in corrosion resistance, such as the elemental distribution, grain size, type and size of second phases. Generally, the methods for improving the corrosion resistance of Mg−Li alloys include alloying and plastic deformation. Al is the common alloying element. Its addition increases the hydrogen evolution overpotential and inhibits the corrosion of alloys [6]. It was reported that dense and compact corrosion products were formed on the corrosion surface of Mg−Li alloys containing high Al element, and further restrained the occurrence of corrosion [7]. Besides, a small amount of Zn element with a relatively high standard electrode potential (−0.76 V, vs SHE), rarely forming a second phase with the other elements in Mg−Li−Al alloy, is beneficial to the potential of the matrix [8]. An appropriate addition of yttrium (Y), as the commonly added rare earth element (RE), can

Corresponding author: Guo-hua WU, Tel: +86-21-54742630, Fax: +86-21-34202794, E-mail: ghwu@sjtu.edu.cn;
Wen-cai LIU, E-mail: liuwc@sjtu.edu.cn
DOI: 10.1016/S1003-6326(21)65783-7

improve the corrosion resistance of Mg alloys [9−11]. XU et al [12] investigated the corrosion behavior of Mg−10.95Li−3.29Al−0.59Y−0.19Zr with a single β-Li matrix. They found that this alloy possessed excellent corrosion resistance. Hot extrusion can refine the microstructure and grain size, thus decreasing the corrosion rate of Mg−Li alloys [13].

There are several reports about the effect of Li content on the corrosion resistance of Mg−Li based alloys. Some reports [8,14,15] indicated that the corrosion resistance decreased in the following order: α-Mg+β-Li alloy, α-Mg alloy, and β-Li alloy. LI et al [16] suggested that the β-Li alloy displayed the lowest corrosion rate followed by the α-Mg alloy, and the α-Mg+β-Li alloy possessed the largest corrosion rate. LIU et al [17] found that the corrosion rate increased in the order of β-Li > α-Mg+β-Li alloy > α-Mg alloys. The differences about the influence of Li content on the corrosion resistance of Mg alloys is attributed not only to the Li content, but also to the elemental distribution, type and size of second phases, and the property of oxide film, and so on.

In this work, Mg−xLi−3Al−2Zn−0.5Y alloys (x=4, 8, 12) were prepared using vacuum melting method, then homogenized and hot extruded. The influence of Li content on the microstructure and corrosion behavior was analyzed, including the type and size of the formed second phases, and the oxide film.

2 Experimental

Pure Mg (99.9 wt.%), pure Li (99.9 wt.%), pure Al (99.9 wt.%), pure Zn (99.9 wt.%) and Mg−20 wt.%Y master alloy were used as raw materials. A vacuum induction furnace with the protection of pure argon gas was used to melt these metals at 730 °C for 10 min. Then, the melts were poured into a stainless steel mold with a diameter of 68 mm. After being cooled to room temperature, the as-cast ingots were obtained. The actual chemical compositions and density of the as-cast LAZx32-0.5Y (x=4, 8, 12, wt.%) alloys (Table 1) were tested by inductively coupled plasma atomic spectroscopy (ICP-AES, Perkin Elmer Plasma−400) and Archimedes method, respectively. Then these ingots were homogenized at 350 °C for 4 h, and the as-homogenized samples were obtained. After the surface oxide film was removed, these homogenized samples were heated at 275 °C for 20 min, and then hot extruded with an extrusion ratio of 16:1. The extruded bar (as-extruded sample) with a diameter of 15 mm was obtained.

The phase identification was carried out using an X-ray diffractometer (XRD, D/Max 2500) with Cu K_α radiation and a scanning rate of 4 (°)/min in the 2θ range of 20°−80°. The microstructures of the samples were observed with a scanning electron microscope (SEM, Quanta−200) equipped with an energy dispersive spectroscope (EDS).

The immersion and electrochemical tests were performed in a 3.5% NaCl solution at room temperature. The hydrogen evolution test was conducted using a fishing-line method, similar to Ref. [18], and the released hydrogen gas was recorded at a regular immersion interval. After immersing for 7 d, the surface corrosion products were removed using 180 g/L chromic acid solution. After being cleaned with alcohol and dried with a cool wind, the mass loss change was obtained and the corrosion morphology after removing the corrosion products was observed using SEM. The potentiodynamic polarization curves were measured on an IM6ex electrochemistry workstation using a classical three electrode cell (samples as working electrode, saturated calomel electrode (SCE) as reference electrode and Pt sheet as counter electrode). The tested samples were inset using resin with an exposed area of 10 mm^2, and the scanning rate was set at 1 mV/s and the scanning potential ranged from −1.95 V to −1.30 V (vs SCE).

Table 1 Actual chemical compositions and density of as-cast LAZx32-0.5Y (x=4, 8, 12) alloys

Alloy	Density/(g·cm^{-3})	Actual composition/wt.%					
		Li	Al	Zn	Y	Fe	Mg
LAZ432-0.5Y	1.631	4.05	3.08	2.27	0.35	0.0033	Bal.
LAZ832-0.5Y	1.532	7.73	3.53	2.09	0.45	0.0051	Bal.
LAZ1232-0.5Y	1.365	12.3	3.35	2.12	0.63	0.0039	Bal.

3 Results

3.1 Microstructure

Figure 1 displays the XRD patterns of the as-homogenized and as-extruded LAZ*x*32-0.5Y alloys (*x*=4, 8, 12). The as-homogenized and as-extruded LAZ432-0.5Y alloys are mainly composed of *α*-Mg, AlLi and Al_2Y phases (see Table 2). In addition to the three phases, two kinds of *β*-Li and $MgLi_2Al$ new phases are detected when the Li content increases to 8%. As the Li content increases to 12%, the diffraction peaks of *α*-Mg phase disappear and the as-homogenized and as-extruded LAZ432-0.5Y alloys mainly consist of *β*-Li, AlLi, Al_2Y and $MgLi_2Al$ phases. According to the binary Mg−Li phase diagram [19], when the Li content is less than 5.7%, the matrix of Mg−Li alloy is *α*-Mg phase with HCP structure. When the Li content exceeds 10.3%, the matrix transforms into

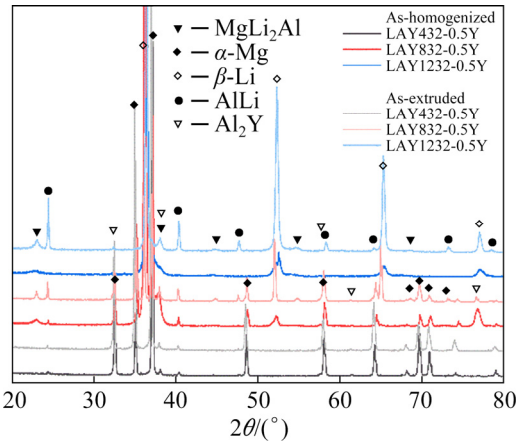

Fig. 1 XRD patterns of as-homogenized and as-extruded LAZ*x*32-0.5Y alloys (*x*=4, 8, 12)

Table 2 Phases of as-homogenized and as-extruded LAZ*x*32-0.5Y (*x*=4, 8, 12) alloys

Alloy	State	Phases
LAZ432-0.5Y	As-homogenized	*α*-Mg, AlLi, Al_2Y
	As-extruded	*α*-Mg, AlLi, Al_2Y
LAZ832-0.5Y	As-homogenized	*α*-Mg, *β*-Li, AlLi, Al_2Y, $MgLi_2Al$
	As-extruded	*α*-Mg, *β*-Li, AlLi, Al_2Y, $MgLi_2Al$
LAZ1232-0.5Y	As-homogenized	*β*-Li, AlLi, Al_2Y, $MgLi_2Al$
	As-extruded	*β*-Li, AlLi, Al_2Y, $MgLi_2Al$

β-Li phase with BCC structure. When the Li content is 5.7%−10.3%, the matrix is composed of (*α*-Mg+*β*-Li) diphase structure. The XRD results are consistent with the rule of binary Mg−Li phase diagram. Besides, the diffraction peaks of AlLi and Al_2Y phases exist in these six alloys, where the peak intensity of AlLi phase is relatively weak. Meanwhile, the diffraction peak of $MgLi_2Al$ phase appears in the as-homogenized/as-extruded LAZ832-0.5Y and LAZ1232-0.5Y alloys, while the peak intensity of as-homogenized LAZ832-0.5Y alloy is relatively weak.

Figure 2 shows the SEM images of as-homogenized and as-extruded LAZ*x*32-0.5Y alloys (*x*=4, 8, 12). The matrix of the as-homogenized LAZ432-0.5Y alloy is light grey *α*-Mg, and some filamentous and irregular white phases are discontinuously distributed along the grain boundaries. According to Ref. [20], the filamentous AlLi phase can exist in the Mg−Li alloy in the form of eutectic combined with *α*-Mg phase. The as-homogenized LAZ432-0.5Y alloy mainly consists of light grey blocky *α*-Mg and deep grey *β*-Li phase. In the magnified image of Fig. 2(b), some irregular bright particles are distributed in the *α*-Mg and *β*-Li phases. The matrix of the as-homogenized LAZ1232-0.5Y alloy is deep grey *β*-Li phase. Relatively big irregular bright particles are discontinuously precipitated along the grain boundaries, and deep grey fine granular particles mainly within the grains. Similar to the as-homogenized alloys, as the Li content increases from 4% to 12%, the matrix of the as-extruded LAZ*x*32-0.5Y alloys transfers from single *α*-Mg phase, (*α*-Mg+*β*-Li) dual phase to single *β*-Li phase. In the as-extruded LAZ432-0.5Y alloy, irregular bright phases are broken into fine particles and distributed along the extrusion direction. The light grey block-like *α*-Mg phases in the as-extruded LAZ832-0.5Y alloy are elongated along the extrusion direction, and a lamellar microstructure is formed. In the magnified image of Fig. 2(e), grey tiny particles are discontinuously distributed along the grain boundaries of *β*-Li phase in the as-homogenized LAZ1232-0.5Y alloy. In the as-homogenized and as-extruded LAZ1232-0.5Y alloys, submicron dark grey globular particles are discontinuously distributed in the *β*-Li phase.

The elemental distribution maps of the as-homogenized and as-extruded LAZ*x*32-0.5Y

(x=4, 8, 12) alloys are shown in Figs. 3 and 4, respectively. For the as-homogenized LAZ432-0.5Y alloy, the eutectic discontinuously distributed along the grain boundary is enriched in Al element. Combined with the previous analysis, the filamentous phase can be identified as AlLi phase. Few irregular bright particles (approximately 2 μm) are mainly composed of Al and Y, inferred as Al_2Y phase. Combined with the XRD results, in the as-extruded LAZ832-0.5Y alloy, most Al_2Y particles are distributed along the phase boundaries between the α-Mg and β-Li phases, and the fine dark grey rich-Al particles in the β-Li matrix (the size below 1 μm) are considered as AlLi phase. In the as-homogenized LAZ1232-0.5Y alloy, the bright particles (2−5 μm in diameter) distributed in the grains and discontinuously distributed along the grain boundaries are mainly composed of Al element, inferred as AlLi phase. The grey tiny particles along the grain boundaries of β-Li phase

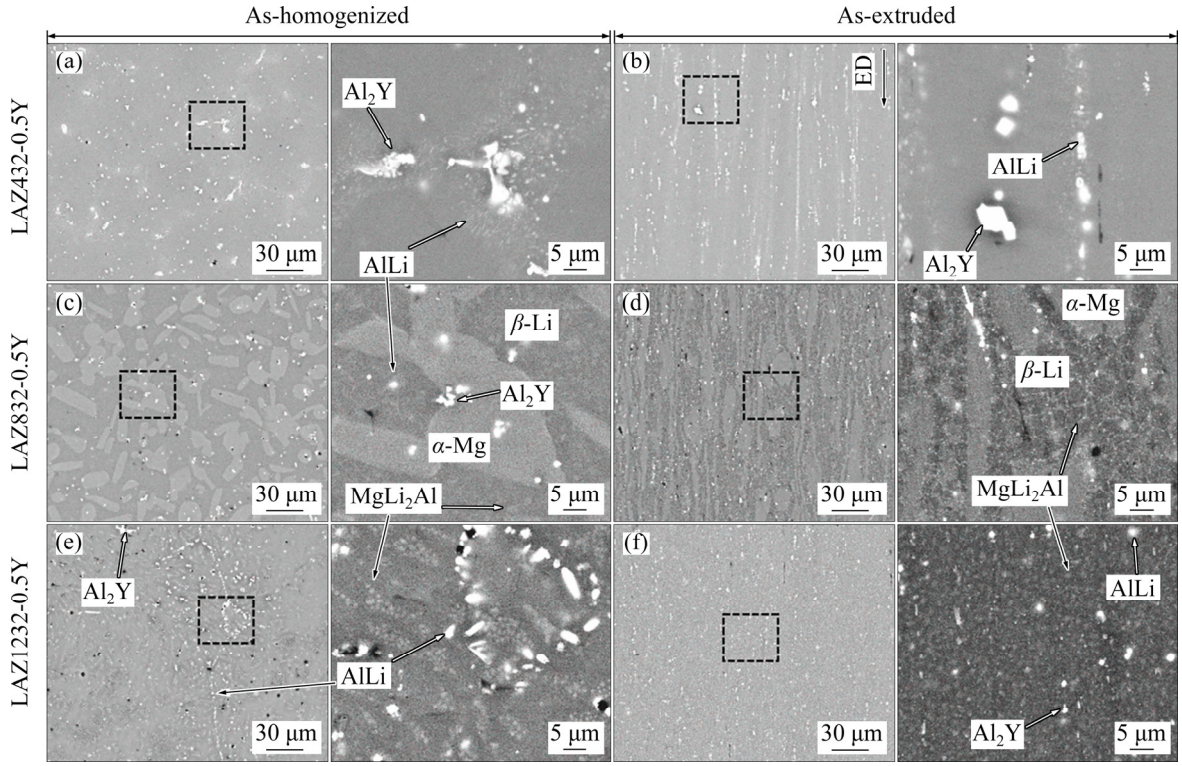

Fig. 2 SEM images of as-homogenized (a) and as-extruded (b) LAZ432-0.5Y alloys, as-homogenized (c) and as-extruded (d) LAZ832-0.5Y alloys, and as-homogenized (e) and as-extruded (f) LAZ1232-0.5Y alloys

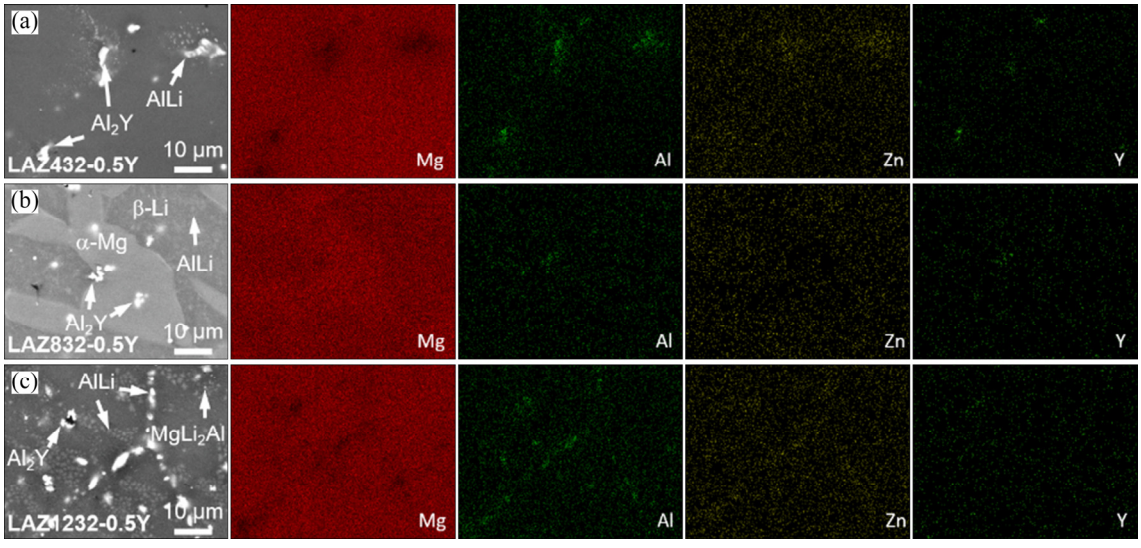

Fig. 3 EDS elemental mappings of as-homogenized LAZx32-0.5Y alloys (x=4, 8, 12)

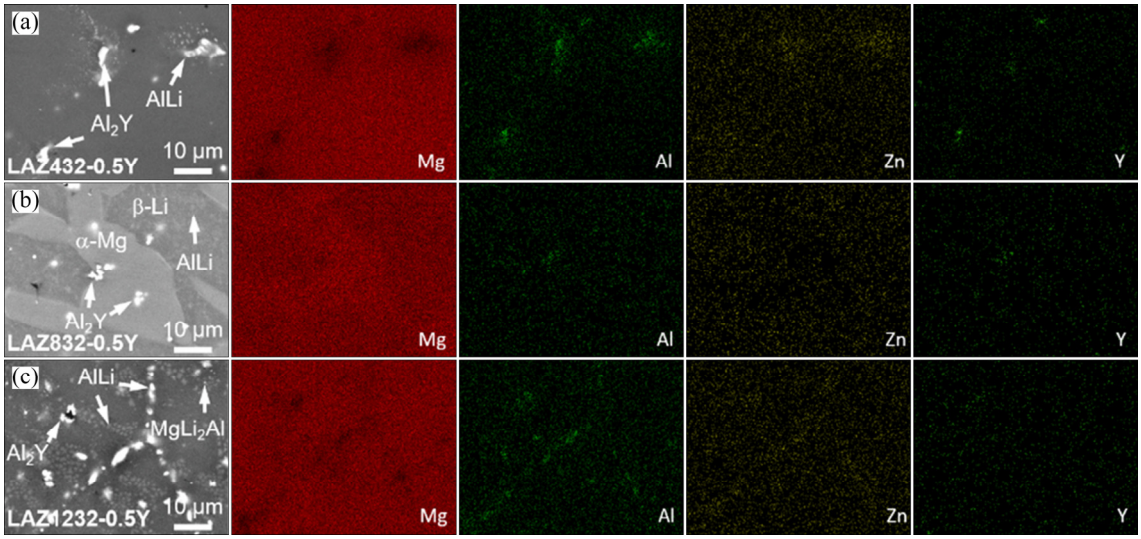

Fig. 4 EDS elemental mappings of as-extruded LAZ*x*32-0.5Y alloys (*x*=4, 8, 12)

are $MgLi_2Al$ phase, which is generally precipitated from the *β*-Li phase during heat treatment or hot extrusion. No Zn-containing phase can be found in the three as-homogenized alloys from the XRD patterns. Therefore, Zn atoms exist in the form of solid solution, which is mainly attributed to the high solubility of Zn in Mg and Li [21].

In the as-extruded LAZ*x*32-0.5Y (*x*=4, 8, 12) alloys, amounts of broken finer bright particles are discontinuously distributed along the extrusion direction, and the corresponding EDS elemental mappings indicate that these phases are enriched in elements Al and/or Y. Combined with the XRD results, these broken particles are AlLi and/or Al_2Y phases. In the as-extruded LAZ832-0.5Y and LAZ1232-0.5Y alloys, nondirectional submicron grey particles are dispersedly distributed along the grain boundaries of *β*-Li phase and enriched in Al element. Combined with the XRD results and Ref. [22], they can be identified as $MgLi_2Al$ ternary phase. The difference of $MgLi_2Al$ and AlLi phase in Fig. 4(c) is that the brightness of the former is slightly higher than that of the latter, and the size of the former is much smaller than that of the latter.

3.2 Corrosion behavior

Figure 5 shows the hydrogen evolution and mass loss rates of the as-homogenized and as-extruded LAZ*x*32-0.5Y alloys (*x*=4, 8, 12) immersed in 3.5% NaCl solution for 7 d. From Figs. 5(a) and (b), the released hydrogen volume increases with the immersion time. The LAZ1232-0.5Y alloy display the highest hydrogen evolution and mass loss rates, and the LAZ432-0.5Y alloy keeps lower hydrogen evolution and mass loss rates. The released hydrogen gas and mass loss rate of the LAZ832-0.5Y alloys are the lowest among these Mg alloys with different Li contents. Generally, the hydrogen volume can be used to reflect the dissolution rate of Mg and its alloys and to evaluate the corrosion rate, because the released hydrogen gas is produced by the cathode hydrogen evolution reaction (HER) [16]. Therefore, a higher hydrogen volume rate means a higher corrosion rate in Mg and its alloys. As a whole, the corrosion resistance of those six alloys decreases as follows: as-extruded LAZ832-0.5Y > as-homogenized LAZ832-0.5Y > as-extruded LAZ432-0.5Y > as- homogenized LAZ432-0.5Y > as-homogenized LAZ1232-0.5Y > as-extruded LAZ1232-0.5Y. The mass loss rate can directly reflect the corrosion rate of Mg and its alloys. According to Fig. 5(c), the sequence of corrosion rate is consistent with the corrosion rate generated by hydrogen evolution rate. The as-homogenized and as-extruded LAZ832-0.5Y alloys show relatively lower mass loss rates of (1.01±0.05) and (0.26±0.11) $mg \cdot cm^{-2} \cdot d^{-1}$, respectively.

The potentiodynamic polarization curves are composed of cathodic branch and anodic branch (see Fig. 6). The former is related to the hydrogen evolution reaction of hydrated protons on the surface of electrode, and the latter is related to the anodic dissolution of Mg alloys. The cathodic corrosion current density (J_{corr}) values fitted from the cathodic branch are listed in Table 3. The J_{corr}

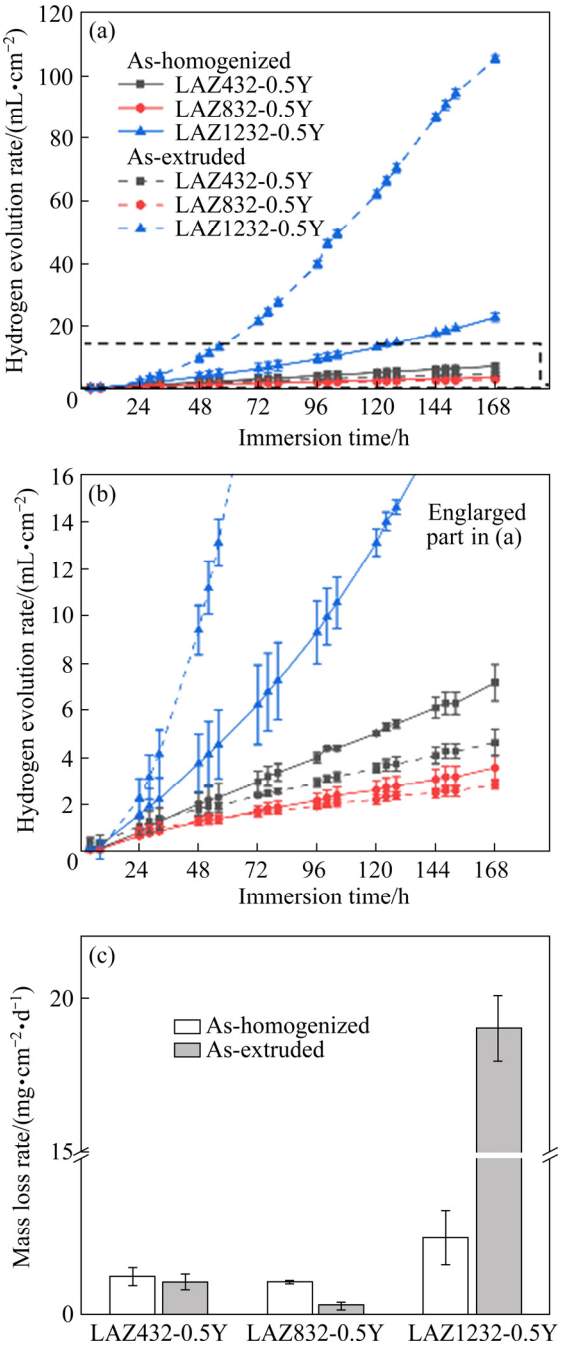

Fig. 5 Hydrogen evolution rate (a, b) and mass loss rate (c) of as-homogenized and as-extruded LAZ*x*32-0.5Y alloys (*x*=4, 8, 12) immersed in 3.5% NaCl solution for 7 d

values of the six alloys increase in the order: as-extruded LAZ832-0.5Y < as-homogenized LAZ832-0.5Y < as-extruded LAZ432-0.5Y < as-homogenized LAZ432-0.5Y < as-homogenized LAZ1232-0.5Y < as-extruded LAZ1232-0.5Y. Generally, a lower J_{corr} value indicates a better corrosion resistance [23,24]. Therefore, the order of corrosion resistance of these alloys is in accordance with the hydrogen evolution and weight loss results.

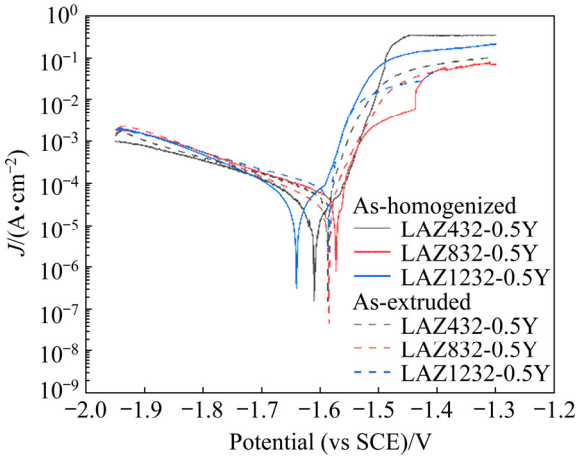

Fig. 6 Potentiodynamic polarization curves of as-homogenized and as-extruded LAZ*x*32-0.5Y alloys (*x*=4, 8, 12) at OCPs

Figure 7 shows the corrosion morphologies of the as-homogenized and as-extruded LAZ*x*32-0.5Y alloys (*x*=4, 8, 12) immersed in 3.5% NaCl solution for 7 d after removing the corrosion products. For the as-homogenized alloys, the corrosion surface of the as-homogenized LAZ432- 0.5Y is uneven, and amounts of large-scale corrosion pits exist in the grains. In the magnified image (Fig. 7(a_2)), the α-Mg phase adjacent to the eutectic along the grain boundaries is preferentially dissolved, and rather deep gullies are formed. Amounts of blocky α-Mg particles are exposed to the surface of the as-homogenized LAZ832-0.5Y alloy. The magnified image (Fig. 7(c_2)) shows that the α-Mg phase adjacent to the large-scale second phase and the β-Li adjacent to the α-Mg phase are preferentially corroded. In Figs. 7(e_1) and (f_1), severe corrosion occurs in the as-homogenized and as-extruded LAZ1232-0.5Y alloys, and obvious corrosion pits and continuous gullies can be observed. In the magnified images (Figs. 7(e_2) and (f_2)), high-density corrosion pits with rough surface occur in the grains. Besides, the tiny globular $MgLi_2Al$ particles are still attached on the corrosion pits of the as-extruded LAZ1232-0.5Y alloy (Fig. 7(f_2)). The corrosion mechanism of the as-homogenized/as-extruded LAZ432-0.5Y and LAZ1232-0.5Y alloys is a mixture of pitting corrosion and intergranular corrosion. This localized selective corrosion along the grain boundaries is called

Table 3 Tafel fitted results from potentiodynamic polarization curves

Alloy	State	φ_{corr}(vs SCE)/V	J_{corr}/(μA·cm^{-2})	β_c/(mV·decade^{-1})
LAZ432-0.5Y	As-homogenized	−1.609	64.5	–217
	As-extruded	−1.587	64.1	–266
LAZ832-0.5Y	As-homogenized	−1.574	44.1	–206
	As-extruded	−1.585	31.9	–175
LAZ1232-0.5Y	As-homogenized	−1.640	70.7	–193
	As-extruded	−1.570	109	–225

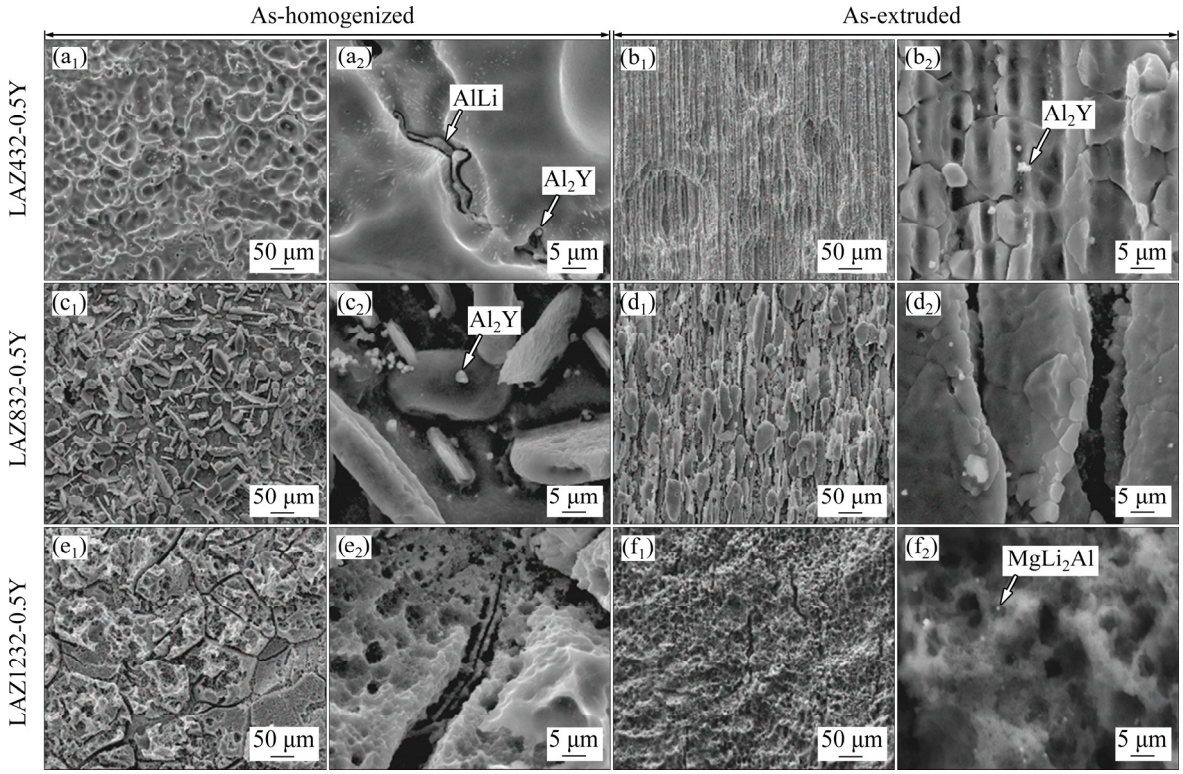

Fig. 7 Corrosion morphologies of samples after immersing in 3.5% NaCl solution for 7 d and removing corrosion products: (a_1, a_2, b_1, b_2) As-homogenized and as-extruded LAZ432-0.5Y; (c_1, c_2, d_1, d_2) As-homogenized and as-extruded LAZ832-0.5Y; (e_1, e_2, f_1, f_2) As-homogenized and as-extruded LAZ1232-0.5Y

intergranular corrosion, and it occurs when the corrosion rate of the grain boundaries exceeds that of the grains. Intergranular corrosion generally occurs in stainless steel [25,26] and wrought Al alloys [27,28], but rarely in Mg alloys [8] due to the negative standard electrode potential of Mg (−2.73 V, vs SHE). It is reported that the AlLi phase possesses a more negative surface potential than the BCC-structure Mg [7,29], thus the AlLi phase distributed along the boundaries is corroded prior to the matrix. Relatively uniform corrosion occurs in the as-extruded LAZ832-0.5Y alloy, elongated α-Mg phase along the extrusion direction is naked on the corrosion surface, and the surrounding β-Li matrix is preferentially dissolved. The magnified image (Fig. 7(d_2)) reveals that slight corrosion occurs along the phase boundaries of α-Mg matrix, while the depth of gullies formed in the β-Li matrix is much larger than that of the former. Hence, the main corrosion of the as-homogenized LAZ832-0.5Y alloy is pitting corrosion, while that of the as-extruded LAZ832-0.5Y alloy is a mixture of pitting corrosion and intergranular corrosion. Figure 8 shows the morphologies of the corrosion products of as-homogenized and as-extruded LAZx32-0.5Y alloys (x=4, 8, 12) immersed in 3.5% NaCl solution for 7 d. The corrosion surface of the as-extruded LAZ832-0.5Y is relatively smooth,

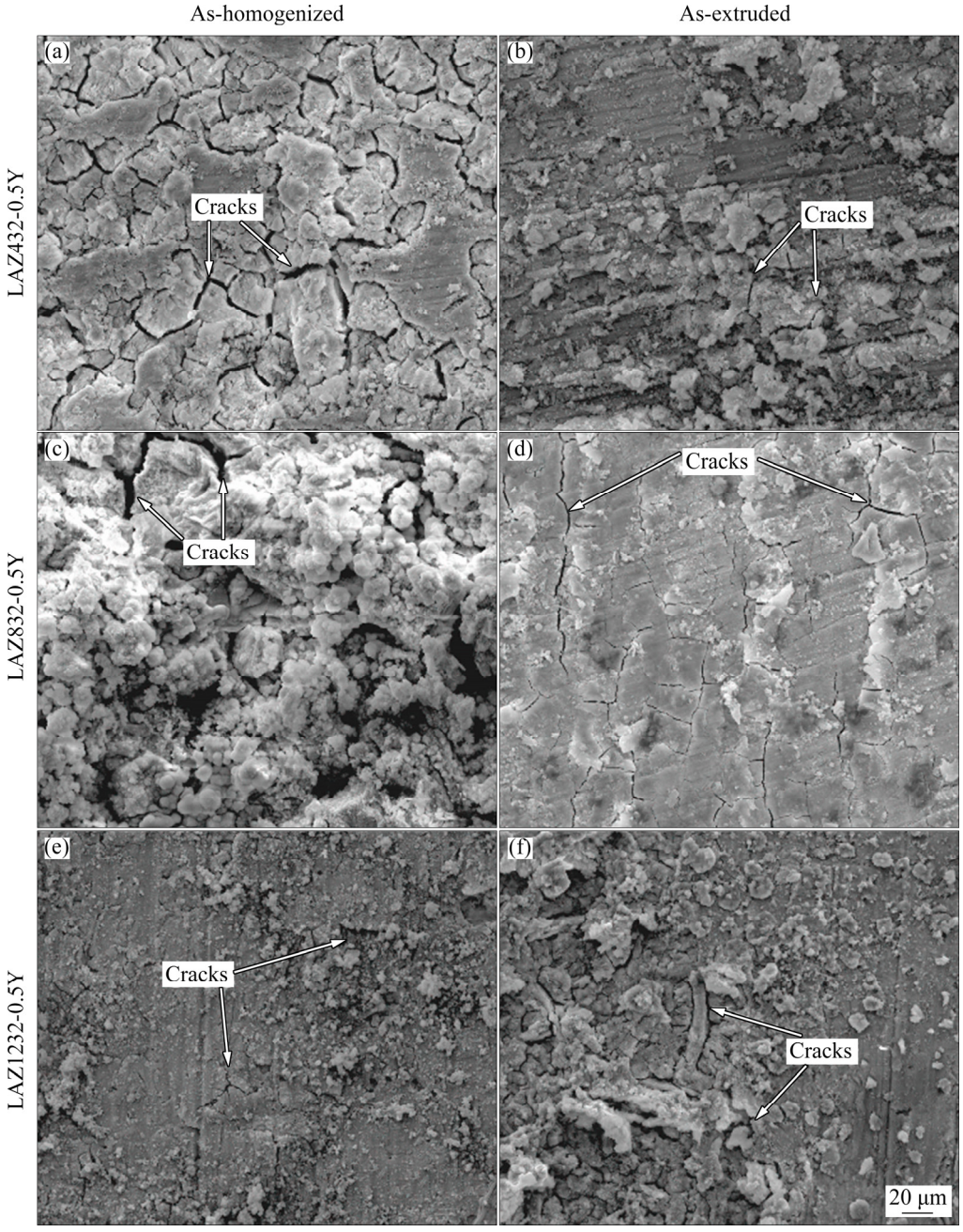

Fig. 8 Morphologies of corrosion products after immersing in 3.5% NaCl solution for 7 d: (a, b) As-homogenized and as-extruded LAZ432-0.5Y; (c, d) As-homogenized and as-extruded LAZ832-0.5Y; (e, f) As-homogenized and as-extruded LAZ1232-0.5Y

while amounts of corrosion products cover on the surface of the other alloys and some cracks exist in the corrosion products of all alloys.

4 Discussion

For Mg−Li alloys, the Li content has a significant influence on the phase components. As analyzed above, 4% Li addition leads to a single α-Mg matrix, 12% Li a single β-Li matrix and 8% Li an (α-Mg+β-Li) diphase matrix in the Mg−Li based alloys. In Y-containing Mg−Li−Al alloys, the Al_2Y phase precipitates in the matrix because of the relatively large electronegativity difference between Al and Y than the other elements (such as Mg and Li) [30].

In the as-homogenized LAY432-0.5Y alloy, a large amount of AlLi phase is discontinuously precipitated along the grain boundaries in the form of eutectic. Therefore, discontinuously distributed

AlLi phase can be found along the grain boundaries of the as-homogenized LAZ432-0.5Y and LAZ1232-0.5Y alloys. In the as-homogenized LAY432-0.5Y and LAY1232-0.5Y alloys, irregular Al_2Y phase is mainly distributed in the grains. But in the as-homogenized LAY832-0.5Y alloy, Al_2Y phase is mainly distributed along the phase interface between the α-Mg and β-Li phases. $MgLi_2Al$ ternary phase generally precipitates from the β-Li phase during heat treatment or hot-extrusion process [22]. In Figures 2(b)−(f), fine granular $MgLi_2Al$ exists in the β-Li matrix of the as-homogenized/as-extruded LAY832-0.5Y and LAY1232-0.5Y alloys.

For the as-homogenized alloys, the Li content changes the phase components. Relatively large-scale irregular Al_2Y and AlLi phases exist in the three kinds of alloys with different Li contents. AlLi phase is mainly distributed along the grain boundaries of the matrix. Besides, $MgLi_2Al$ phase only exists in the as-homogenized/as-extruded LAY832-0.5Y and LAY1232-0.5Y alloys. After hot extrusion, the phase type has no obvious change according to the XRD results, while the size and volume fraction are different. For the as-extruded alloys, the Al_2Y and AlLi phases are crashed into smaller size, and the blocky α-Mg phase of the LAY832-0.5Y alloy is elongated along the extrusion direction.

The poor corrosion resistance of Mg and its alloys is mainly attributed to the negative potential and non-protective oxide/hydroxide film [31]. For Mg alloys, the microstructure plays a significant role in the corrosion behavior, including second phase, elemental distribution and texture. Generally, potential difference between the second phase and the Mg matrix can be formed. According to the electrochemistry theory, galvanic corrosion will occur because the two phases have potential difference in solution. Cathode may be precipitates, impurities in Mg alloy or other metals in contact with Mg in the electrolyte. As well known, the standard electrode potential of Li (−3.02 V, vs SHE) is more negative than that of Mg (−2.37 V, vs SHE), and thus the chemical activity of Li is higher than that of Mg. In dual phase Mg−Li alloys, the chemical activity of β-Li phase is higher than that of α-Mg phase because of the higher Li content in the β-Li phase than in the α-Mg phase. Hence, micro-galvanic corrosion occurs because of the potential difference between the α-Mg and β-Li phases, and the β-Li phase as the micro cathode is preferentially dissolved. In Figs. 7(a_2)−(c_2), the α-Mg phase near the Al_2Y particles is preferentially corroded, and thus the surface potential of Al_2Y phase is higher than that of α-Mg phase. Combined with the previous reports [7,29], we can get that the surface potentials decrease in the order: Al_2Y, α-Mg > β-Li, and AlLi. Besides, it is reported that the $MgLi_2Al$ ternary phase possesses a higher surface potential than the β-Li phase. Therefore, in Mg−Li alloys containing β-Li phase, the large potential difference between the $MgLi_2Al$ and β-Li phases induces a micro-galvanic corrosion and the $MgLi_2Al$ phase acts as the micro cathode. Zn has a higher standard electrode potential (–0.76 V, vs SHE) than Al (–1.67 V, vs SHE). In this work, Zn atoms are mainly dispersed in the matrix in the form of solid solution, which is beneficial to improving the potential of the matrix.

Figure 9 shows the corrosion rates (P_H, P_W, P_J, mm/a) calculated by formulas in Refs. [32−34] from hydrogen evolution, mass loss rate and cathodic corrosion current density. According to the corrosion rates, the corrosion resistance of the six alloys can be ranked in an decreasing order as: as-extruded LAZ832-0.5Y > as-homogenized LAZ832-0.5Y > as-extruded LAZ432-0.5Y > as-homogenized LAZ432-0.5Y > as-homogenized LAZ1232-0.5Y > as-extruded LAZ1232-0.5Y alloy. The as-homogenized/as-extruded LAZ1232-0.5Y alloys with the highest Li content display a larger corrosion rate, and the dual phase LAZ832-0.5Y

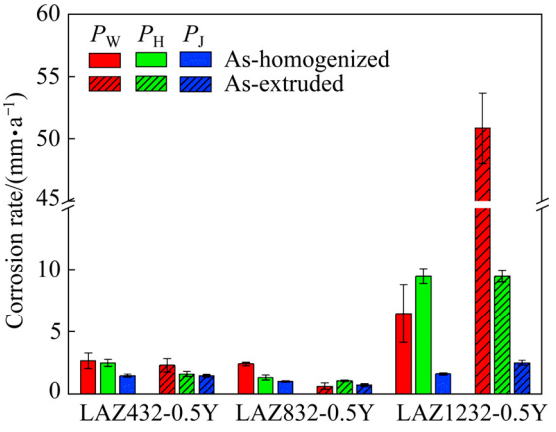

Fig. 9 Corrosion rates (P_W, P_H, P_J) of as-homogenized and as-extruded LAZx32-0.5Y (x=4, 8, 12) alloys according to mass loss rate, hydrogen evolution and cathodic corrosion current density

alloys possess a smaller corrosion rate. Among them, the corrosion resistance of the as-extruded LAZ832-0.5Y alloy is the best (P_W=(0.63±0.26) mm/a).

Al_2Y and AlLi phases exist in all tested alloys, and micro-galvanic corrosion easily occurs at the interface between the second phases and the matrix. Especially, the AlLi phase with a more negative potential has a negative impact on the corrosion resistance of Mg−Li alloys, and the relatively large potential difference between the large-scale Al_2Y phase and the matrix accelerates the corrosion process. As for the dual phase Mg−Li alloy, the surface potential of α-Mg is between those of the Al_2Y and β-Li phases, and thus can weaken the potential difference of Al_2Y and β-Li phases. Besides, the β-Li phase is preferentially dissolved, and the blocky α-Mg phase with high volume fraction retains in the matrix. Therefore, the corrosion resistance of the alloy can be improved through sacrificing the β-Li phase to protect the α-Mg phase. The corrosion resistance of the as-extruded LAZ432-0.5Y and LAZ832-0.5Y alloys is higher than that of the corresponding as-homogenized alloys, which is related to the size and distribution of second phases. In the as-homogenized alloys, large scale second phases would induce severe micro-galvanic corrosion because of a large electrochemical inhomogeneity of alloys. After hot extrusion, finer and more uniform distribution of second phases in the LAZ432-0.5Y and LAZ832-0.5Y alloys is beneficial to the improvement of whole electrochemical homogeneity. However, the corrosion rate of the as-homogenized LAZ1232-0.5Y alloy is higher than that of as-extruded one, which is related to the more precipitated tiny $MgLi_2Al$ particles from the β-Li phase and the residual stress after hot extrusion. In Fig. 7(f_2), the large potential difference between the $MgLi_2Al$ and β-Li phases induces micro-galvanic corrosion, and more $MgLi_2Al$ particles deteriorate the dissolution of β-Li phase. It is reported that amounts of sub-grains are easily found in the β-Li phase although dynamic recrystallization (DRX) occurs in the β-Li phase because the stacking faulting energy of Mg is lower than that of Li [22,35,36]. Therefore, the dislocations on the sub-grain boundaries would accelerate the anode dissolution of the matrix [37].

The surface oxide film property of Mg and its alloys also has an important effect on the corrosion behavior. The stability and protectiveness of surface oxide covered on the metals mainly depend on the standard enthalpy of relevant compounds, Pilling-Bedworth ratio (PBR) and solubility in solution [8,38,39]. Among them, the standard enthalpy of relevant compounds indicates the chemical stability. More negative standard enthalpy has greater tendency of compound formation. The PBR value can describe the property and compactness of the surface oxide film on metals. When the PBR value is below 1 or beyond 2, relatively small tensile stress or great compressive stress is generated on the surface oxide film, and loose or cracked oxide film is not conducive to the protection of the internal metal. When the PBR value is in the range of 1−2, the appropriate compressive stress between the oxide film and metal is beneficial to inhibiting further corrosion. For the formed oxide film, the stability is closely connected to the solubility in solution. When the solubility of compound in solution is large, the compound easily dissolved in water is harmful to the protectiveness of inner metal.

The alloy surface of Mg−Li alloys with higher chemical activities can naturally react with oxygen in air, and oxides of magnesium and lithium are formed. The PBR values of MgO and Li_2O are 0.8 and 0.57 (<1), respectively [38], and thus the loose structure of oxide film promotes the permeation of solution in the inner. Meanwhile, the oxides react with water and/or carbon dioxide, and corresponding carbonic acid and/or hydroxides are formed. Among them, the standard enthalpy of Li_2CO_3 is more negative than that of Li_2O, and the formation tendency of Li_2CO_3 is larger. The PBR values of Li_2CO_3 and LiOH generated by chemical reaction and electrochemical reaction are 1.26 and 1.35 (in the range of 1−2), respectively [38], and beneficial to the formation of a compact film. However, their solubility values in 100 g water are 12.8 g·and 1.33 g (at 20 °C), respectively, and the large solubility in water is not conducive to the formation of a dense film. The PBR value of $MgCO_3$ is 2.04, and thus the compound easily cracks and spalls off. As the main component of corrosion products of Mg and its alloys, although $Mg(OH)_2$ displays an appropriate PBR value (1.80) and low solubility value in water, its structure is

loose and porous, and can be passed through by chloride ions with a small radius, thus having a limited protective effect on the alloy.

As a whole, because of the physical/chemical instability of oxides, hydroxides and carbonates formed in Mg−Li alloys, the surface oxide film formed is not dense, which is not conducive to effective protection of the alloys. As shown in Figs. 8(a)−(f), loose and porous corrosion products have many cracks, and their distribution is not uniform, which limits protecting the inner alloy in a long-term immersion. Besides, an amount of hydrogen gas produced by the electrochemical reaction escaping from the corrosion pits leads to the crack of oxide film, and the formed hydrogen poles act as channels to connect the corrosive medium to the metal matrix, thus accelerating further corrosion. Even though, the integrity of oxide film on the surface of as-extruded LAZ832-0.5Y alloy is higher than that of the others, indicating the oxide film has a protective effect on the alloy to some degree.

Summarizing the above analysis, the superior corrosion resistance of as-extruded LAZ832-0.5Y alloy can be mainly attributed to the following factors. First, after hot extrusion finer second phases and their more uniform distribution weaken the local potential difference between the second phases and the matrix, and decrease the driving force of local corrosion. Second, although in the dual phase LAZ832-0.5Y alloy the potential difference between the α-Mg and β-Li phases induces the micro-galvanic corrosion, the rather large-scale blocky α-Mg phase as micro-anode is retained in the matrix. In other words, the α-Mg phase can be protected via sacrificing the micro-cathodic β-Li phase in the corrosion process. Third, although the components of corrosion products on the surface of Mg−Li alloys possess chemical/physical instability, relatively integrated oxide film formed on the surface of as-extruded LAZ832-0.5Y alloy can protect the alloys from further corrosion to some degree (Fig. 8(d)).

5 Conclusions

(1) The Li addition in Mg alloys changes the matrix from single α-Mg phase, dual phase (α-Mg+β-Li) to single β-Li phase. When the Li content increases to 8% and 12%, tiny $MgLi_2Al$ phase is discontinuously precipitated along the grain boundaries of β-Li phase.

(2) A mixed corrosion feature of pitting corrosion and intergranular corrosion mainly occurs in the LAZ432-0.5Y and LAZ1232-0.5Y alloys, which is related to the AlLi phase of negative-potential discontinuously precipitated along the grain boundaries and high potential difference between the second phases and the matrix.

(3) The corrosion resistance of the LAZ832-0.5Y alloys is better than that of single α-Mg/β-Li phase LAZ432-0.5Y and LAZ1232-0.5Y alloys. Hot extrusion is beneficial to decrease the corrosion rate of the LAZ432-0.5Y and LAZ832-0.5Y alloys but accelerate the corrosion of the LAZ1232-0.5Y alloy.

(4) The as-extruded LAZ832-0.5Y alloy displays a superior corrosion resistance with the lowest corrosion rate of (0.63±0.26) mm/a (P_W), which is attributed to the more uniform distribution of second phases, the protective α-Mg phase via sacrificing the β-Li phase and the relatively integrated oxide film.

Acknowledgments

This study was financially supported by the National Natural Science Foundation of China (Nos. 51771115, 51775334, 51821001, U2037601) and Open Fund of State Key Laboratory of Advanced Forming Technology and Equipment (No. SKL2020005).

References

[1] LIU Xu-he, ZHAN Hai-bo, GU Shi-hai, QU Zhi-kun, WU Rui-zhi, ZHANG Mi-lin. Superplasticity in a two-phase Mg−8Li−2Zn alloy processed by two-pass extrusion [J]. Materials Science and Engineering A, 2011, 528(19−20): 6157−6162.

[2] PENG Xiang, LIANG Xin-li, LIU Wen-cai, WU Guo-hua, JI Hao, TONG Xin, ZHANG Liang, DING Wen-jiang. High-cycle fatigue behavior of Mg−8Li−3Al−2Zn−0.5Y alloy under different states [J]. Journal of Magnesium and Alloys, 2021, 9(5): 1609−1618.

[3] AL-SAMMAN T. Comparative study of the deformation behavior of hexagonal magnesium−lithium alloys and a conventional magnesium AZ31 alloy [J]. Acta Materialia, 2009, 57(7): 2229−2242.

[4] ESMAILY M, SVENSSON J E, FAJARDO S, BIRBILIS N, FRANKEL G S, VIRTANEN S, ARRABAL R, THOMAS S, JOHANSSON L G. Fundamentals and advances in magnesium alloy corrosion [J]. Progress in Materials Science, 2017, 89: 92−193.

[5] LI Chuan-qiang, HE Yi-bin, HUANG Huai-pei. Effect of lithium content on the mechanical and corrosion behaviors of HCP binary Mg−Li alloys [J]. Journal of Magnesium and Alloys, 2021, 9: 569−580.

[6] MORISHIGE T, OBATA Y, GOTO T, FUKAGAWA T, NAKAMURA E, TAKENAKA T. Effect of Al Composition on the corrosion resistance of Mg−14 mass% Li system alloy [J]. Materials Transactions, 2016, 57(10): 1853−1856.

[7] WANG B J, XU D K, CAI X, QIAO Y X, SHENG L Y. Effect of rolling ratios on the microstructural evolution and corrosion performance of an as-rolled Mg−8wt.%Li alloy [J]. Journal of Magnesium and Alloys, 2021, 9: 560−568.

[8] SUN Yue-hua, WANG Ri-chu, PENG Chao-qun, CAI Zhi-yong. Microstructure and corrosion behavior of as-extruded Mg−*x*Li−3Al−2Zn−0.2Zr alloys (*x*=5, 8, 11 wt.%) [J]. Corrosion Science, 2020, 167: 108487.

[9] LIU Wen-cai, FENG Shi, LI Zhong-quan, ZHAO Jiong, WU Guo-hua, WANG Xian-fei, XIAO Lv, DING Wen-jiang. Effect of rolling strain on microstructure and tensile properties of dual-phase Mg−8Li−3Al−2Zn−0.5Y alloy [J]. Journal of Materials Science and Technology, 2018, 34: 2256−2262.

[10] PENG Xiang, XU Shi-hao, DING De-hua, LIAO Guang-lan, WU Guo-hua, LIU Wen-cai, DING Wen-jiang. Microstructural evolution, mechanical properties and corrosion behavior of as-cast Mg−5Li−3Al−2Zn alloy with different Sn and Y addition [J]. Journal of Materials Science and Technology, 2021, 72: 16−22.

[11] ZHAO Jiong, ZHANG Jie, LIU Wen-cai, WU Guo-hua, ZHANG Liang. Effect of Y content on microstructure and mechanical properties of as-cast Mg−8Li−3Al−2Zn alloy with duplex structure [J]. Materials Science and Engineering A, 2016, 650: 240−247.

[12] XU W Q, BIRBILIS N, SHA G, WANG Y, DANIELS J E, XIAO Y, FERRY M. A high-specific-strength and corrosion-resistant magnesium alloy [J]. Nature Materials, 2015, 14(12): 1229-35.

[13] LIANG Xin-li, PENG Xiang, JI Hao, LIU Wen-cai, WU Guo-hua, DING Wen-jiang. Microstructure and mechanical properties of as-cast and solid solution treated Mg−8Li−*x*Al−*y*Zn alloys [J]. Transactions of Nonferrous Metals Society of China, 2021, 31(4): 925−938.

[14] OUYANG Si-jie, LIU Wen-cai, WU Guo-hua, JI Hao, GAO Zhan-kui, PENG Xiang, LI Zhong-quan, DING Wen-jiang. Microstructure and mechanical properties of as-cast Mg−8Li−*x*Zn−*y*Gd (*x*=1, 2, 3, 4; *y*=1, 2) alloys [J]. Transactions of Nonferrous Metals Society of China, 2019, 29(6): 1211−1222.

[15] HE Yu-qing, PENG Chao-qun, FENG Yan, WANG Ri-chu, ZHONG Jian-feng. Effects of alloying elements on the microstructure and corrosion behavior of Mg−Li−Al−Y alloys [J]. Journal of Alloys and Compounds, 2020, 834: 154344.

[16] LI C Q, XU D K, CHEN X B, WANG B J, WU R Z, HAN E H, BIRBILIS N. Composition and microstructure dependent corrosion behaviour of Mg−Li alloys [J]. Electrochimica Acta, 2018, 260: 55−64.

[17] LIU Xuan, XUE Ji-lai, LIU Shi-zhe. Discharge and corrosion behaviors of the α-Mg and β-Li based Mg alloys for Mg-air batteries at different current densities [J]. Materials and Design, 2018, 160: 138−146.

[18] SHI Zhi-ming, ATRENS Andrej. An innovative specimen configuration for the study of Mg corrosion [J]. Corrosion Science, 2011, 53(1): 226−246.

[19] MA Xiao-chun, JIN Si-yuan, WU Rui-zhi, WANG Jia-xiu, WANG Gui-xiang, KRIT Boris, BETSOFEN Sergey. Corrosion behavior of Mg−Li alloys: A review [J]. Transactions of Nonferrous Metals Society of China, 2021, 31: 3228−3254.

[20] SUN Yue-hua, WANG Ri-chu, PENG Chao-qun, FENG Yan. Effects of Sn and Y on the microstructure, texture, and mechanical properties of as-extruded Mg−5Li−3Al−2Zn alloy [J]. Materials Science and Engineering A, 2018, 733: 429−439.

[21] LI Chuan-qiang, TONG Zhi-pei, HE Yi-bin, HUANG Huai-pei, DONG Yong, ZHANG Peng. Comparison on corrosion resistance and surface film of pure Mg and Mg−14Li alloy[J]. Transactions of Nonferrous Metals Society of China, 2020, 30(9): 2413−2423.

[22] SUN Yue-hua, WANG Ri-chu, REN Jian, PENG Chao-qun, CAI Zhi-yong. Microstructure, texture, and mechanical properties of as-extruded Mg−*x*Li−3Al−2Zn−0.2Zr alloys (*x*=5, 7, 8, 9, 11 wt.%) [J]. Materials Science and Engineering A, 2019, 755: 201−210.

[23] LIU Xiao-yan, WANG Zhao-peng, FU Bao-gang, LONG Liang, ZHANG Xi-liang, CUI Hao-xuan. Effects of Mg content on the mechanical properties and corrosion resistance of Al−Cu−Mg−Ag alloy [J]. Journal of Alloys and Compounds, 2016, 685: 209−215.

[24] SONG D, MA A B, JIANG J H, LIN P H, YANG D H, FAN J F. Corrosion behaviour of bulk ultra-fine grained AZ91D magnesium alloy fabricated by equal-channel angular pressing [J]. Corrosion Science, 2011, 53(1): 362−373.

[25] HU Chang-liang, XIA Shuang, LI Hui, LIU Ting-guang, ZHOU Bang-xin, CHEN Wen-jue, WANG Ning. Improving the intergranular corrosion resistance of 304 stainless steel by grain boundary network control [J]. Corrosion Science, 2011, 53(5): 1880−1886.

[26] PARDO A, MERINO M C, COY A E, VIEJO F, CARBONERAS M, ARRABAL R. Influence of Ti, C and N concentration on the intergranular corrosion behaviour of AISI 316Ti and 321 stainless steels [J]. Acta Materialia, 2007, 55(7): 2239−2251.

[27] LI Jing-hui, LI Fu-guo, MA Xin-kai, LI Jiang, LIANG Shan. Effect of grain boundary characteristic on intergranular corrosion and mechanical properties of severely sheared Al−Zn−Mg−Cu alloy [J]. Materials Science and Engineering A, 2018, 732: 53−62.

[28] LI Hai, ZHAO Pei-pei, WANG Zhi-xiu, MAO Qing-zhong, FANG Bi-jun, SONG Ren-guo, ZHENG Zi-qiao. The intergranular corrosion susceptibility of a heavily overaged Al−Mg−Si−Cu alloy [J]. Corrosion Science, 2016, 107: 113−122.

[29] GU Mao-yun, WEI Guang-ling, ZHAO Jiong, LIU Wen-cai, WU Guo-hua. Influence of yttrium addition on the corrosion behaviour of as-cast Mg−8Li−3Al−2Zn alloy [J]. Materials Science and Technology, 2016, 33: 864−869.

[30] CUI Chong-liang, WU Li-bin, WU Rui-zhi, ZHANG

Jing-huai, ZHANG Mi-lin. Influence of yttrium on microstructure and mechanical properties of as-cast Mg−5Li−3Al−2Zn alloy [J]. Journal of Alloys and Compounds, 2011, 509(37: 9045−9049.

[31] KIANI Faisal, WEN Cuie, LI Yun-cang. Prospects and strategies for magnesium alloys as biodegradable implants from crystalline to bulk metallic glasses and composites—A review [J]. Acta Biomaterialia, 2020, 103: 1−23.

[32] ATRENS Andrej, SONG Guang-ling, LIU Ming, SHI Zhi-ming, CAO Fu-yong, DARGUSCH Matthew S. Review of recent developments in the field of magnesium corrosion [J]. Advanced Engineering Materials, 2015, 17: 400−453.

[33] KING A D, BIRBILIS N, SCULLY J R. Accurate electrochemical measurement of magnesium corrosion rates; a combined impedance, mass-loss and hydrogen collection study [J]. Electrochimica Acta, 2014, 121: 394−406.

[34] SHI Zhi-ming, LIU Ming, ATRENS Andrej. Measurement of the corrosion rate of magnesium alloys using Tafel extrapolation [J]. Corrosion Science, 2010, 52(2): 579−588.

[35] YANG Yan, PENG Xiao-dong, WEN Hai-ming, ZHENG Bao-long, ZHOU Yi-zhang, XIE Wei-dong, LAVERNIA Enrique J. Influence of extrusion on the microstructure and mechanical behavior of Mg−9Li−3Al−*x*Sr alloys [J]. Metallurgical and Materials Transactions A, 2013, 44(2): 1101−1113.

[36] ZOU Yun, ZHANG Le-hao, WANG Hong-tao, TONG Xin, ZHANG Mi-lin, ZHANG Zhong-wu. Texture evolution and their effects on the mechanical properties of duplex Mg−Li alloy [J]. Journal of Alloys and Compounds, 2016, 669: 72−78.

[37] HAMU G B, ELIEZER D, WAGNER L. The relation between severe plastic deformation microstructure and corrosion behavior of AZ31 magnesium alloy [J]. Journal of Alloys and Compounds, 2009, 468(1): 222−229.

[38] ZENG Rong-chang, SUN Lu, ZHENG Yu-feng, CUI Hong-zhi, HAN En-hou. Corrosion and characterisation of dual phase Mg−Li−Ca alloy in Hank's solution: The influence of microstructural features [J]. Corrosion Science, 2014, 79: 69−82.

[39] WEN Lu, YU Kun, XIONG Han-qing, DAI Yi-long, YANG Shi-hai, QIAO Xue-yan, TENG Fei, FAN Su-feng. Composition optimization and electrochemical properties of Mg−Al−Pb−(Zn) alloys as anodes for seawater activated battery [J]. Electrochimica Acta, 2016, 194: 40−51.

固溶态和挤压态 Mg−*x*Li−3Al−2Zn−0.5Y (*x*=4, 8, 12)合金的显微组织和腐蚀行为

彭 翔，孙家伟，刘宏杰，吴国华，刘文才

上海交通大学 材料科学与工程学院 轻合金精密成型国家工程中心和
金属基复合材料国家重点实验室，上海 200240

摘 要：研究固溶态和挤压态 Mg−*x*Li−3Al−2Zn−0.5Y (*x*=4, 8, 12，质量分数，%)合金的显微组织和腐蚀行为。结果表明，当锂含量从 4%增加到 12%，合金基体由 α-Mg 单相转变为 α-Mg+β-Li 双相，再转变为 β-Li 单相。Mg−4Li−3Al−2Zn−0.5Y 和 Mg−12Li−3Al−2Zn−0.5Y 合金具有晶间腐蚀和点蚀的混合腐蚀特征，前者与沿晶界析出的 AlLi 相有关，后者与第二相与基体之间的高电位差有关。挤压态合金的耐蚀性优于固溶态合金。挤压态 Mg−8Li−3Al−2Zn−0.5Y 合金具有最低腐蚀速率(P_W=(0.63±0.26) mm/a)，主要归因于该合金的第二相分布更均匀、通过牺牲 β-Li 相形成的保护性 α-Mg 相和相对完整的更均匀分布的氧化膜。

关键词：Mg−*x*Li−3Al−2Zn−0.5Y；显微组织；腐蚀行为；固溶；挤压；第二相；氧化膜

(Edited by Sai-qian YUAN)